Colloidal suspensions in modulated light fields

2008 J. Phys.: Condens. Matter 20 404220

(http://iopscience.iop.org/0953-8984/20/40/404220)

IOP Publishing Journal of Physics: Condensed Matter

J. Phys.: Condens. Matter **20** (2008) 404220 (12pp) doi:10.1088/0953-8984/20/40/404220

Colloidal suspensions in modulated light fields

M C Jenkins and S U Egelhaaf

Condensed Matter Physics Laboratory, Lehrstuhl für Physik der weichen Materie,
Heinrich-Heine-Universität Düsseldorf, Universitätstraße 1, D-40225 Düsseldorf, Germany

E-mail: matthew.jenkins@uni-duesseldorf.de

Received 13 May 2008, in final form 17 June 2008
Published 10 September 2008
Online at stacks.iop.org/JPhysCM/20/404220

Abstract

Periodically modulated potentials in the form of light fields have previously been applied to induce reversible phase transitions in dilute colloidal systems with long-range interactions. Here we investigate whether similar transitions can be induced in very dense systems, where inter-particle contacts are important. Using microscopy we show that particles in such systems are indeed strongly affected by modulated potentials. We discuss technical aspects relevant to generating the light-induced potentials and to simultaneously imaging the particles. We also consider what happens when the particle size is comparable to the modulation wavelength. The effects of selected modulation wavelengths as well as pure radiation pressure are illustrated.

(Some figures in this article are in colour only in the electronic version)

1. Introduction

One of the defining features of soft matter systems, their intermediate, or mesoscopic, lengthscale, places them at a remarkable confluence of physical properties, where they are susceptible to influence by 'everyday' external forces. Not only are they 'soft' in their response to applied shear and their constituents sufficiently buoyant to display an interesting interplay between gravity and thermal (Brownian) motion [1], colloids are also affected by the radiation pressure—ordinarily thought of as negligible in laboratory experiments—arising as they scatter light which impinges on them.

The coincidence of the magnitude of these forces (Brownian, gravitational, and that arising from scattered EM radiation) in these systems, set fundamentally by the relative magnitudes of Boltzmann's constant k_b, the gravitational constant G, the speed of light c, and Planck's constant h, is compounded by a coincidence of the particle size with the wavelength of visible light. The remarkable consequence is that we are able to study, in real space, Brownian particles under the influence of light-induced potentials. Ashkin is credited with first realizing this possibility [2–7], leading ultimately to his development of optical tweezers [8]. These are now a widely-used tool in physics [9] and biology [10–12]. Studies using optical tweezers generally consider very deep potential minima, where objects are tightly trapped; the present work considers, in addition, the case where potentials do not necessarily irreversibly capture particles but do bias them towards certain locations.

Colloids have found favour as models of atomic systems, among their advantages being the possibility of imaging directly large colloids with light microscopy, the relatively slow speed at which they diffuse, and the relative ease with which interactions can be tailored [13, 14]. In the apparently simple case of hard-sphere interactions, colloidal systems show the predicted entropy-driven fluid–solid transition at high density [15] and, at higher densities still, a glass transition instead of the expected crystalline equilibrium state, again in analogy with atomic and molecular glass-forming systems [15–19]. Similar behaviour has been seen in other systems, for example charged particles interacting via long-ranged electrostatic repulsion [20].

Fluid–solid transitions are ubiquitous in nature, and are frequently the expected equilibrium state. Often, solid phases occur upon cooling, whereupon distinct density modulations are enhanced, resulting in translational and orientational order. Periodically modulated potentials can have a similar effect, giving rise to a controllable phase transition effected at will by the application and removal of an external potential. Chowdhury was the first to demonstrate this, in two dimensions, in so-called laser-induced freezing (LIF) experiments [21, 22]. These were followed by further experimental [23–26] and theoretical [27–30] confirmation. In LIF, a one-dimensionally modulated potential gives rise to

a two-dimensionally modulated crystal. The registration of adjacent rows is mediated by Brownian motion perpendicular to the direction of the potential, which the particles continue to undergo, although they sit on average at the minima of the potential. For deeper potentials, the lateral motion of the particles becomes sufficiently restricted that the system is only modulated in one dimension, but remains liquid-like along the direction of the fringes; laser-induced melting (LIM) occurs [31–39]. There are many open questions relating to light-induced phase transitions, ranging from the kinetics of LIF and LIM, to as yet untested predictions for systems with more complex inter-particle potentials [40], time-varying potentials [41], and binary mixtures [42].

LIF and LIM both represent transitions between equilibrium states, brought about by the application of external, laser-induced potentials. In each of these cases, removal of the potential leads to a re-establishment of the initial state. In contrast to reversible light-induced transitions, there is the possibility that externally-applied modulated potentials may induce expected but unobserved transitions to ordered states. A prime example is the hard-sphere glass transition described above, though other glass and gel transitions may be relevant. Dynamical arrest due to co-operative effects such as caging is frequently offered as a possible explanation for the glass transition, e.g. [18, 43, 44]. It is known that shear can lead to ordering in glasses and gels [45–49], though the underlying mechanism is still far from understood [50, 51]. (Note that shear can also lead to melting of crystals [52, 53].) If the emerging picture of co-operative arrest is accurate, and given the above evidence of external field-induced ordering, it seems plausible that periodic light fields might also induce ordering in very dense systems. Biroli *et al* have developed an inhomogeneous mode-coupling theory (MCT) which predicts the response of a supercooled liquid's dynamical structure factor when exposed to a static inhomogeneous potential [54]. Agreement of these calculations with experimental results would represent a powerful test for MCT.

This paper describes a first investigation into whether periodically modulated light fields can indeed induce an effect in very dense colloidal systems. In a few initial steps towards the grand goals mentioned above, we present some technical aspects relating to the experimental realization of an apparatus which permits exposure of a sample to the light fields and its simultaneous observation. Our first results with this apparatus show that even the most dense samples do show a clear rearrangement under the influence of an applied light field.

2. Light as an external potential for colloidal particles

Light forces acting on small particles have been described in considerable detail, both from a ray-optics and a Rayleigh perspective. The necessary basic physics is well established [55–58]. We outline the two features most important to the present work, the so-called scattering force F_{scat}, which acts in the direction of beam propagation, and the gradient force F_{grad}, which depends on the shape of the light intensity distribution.

2.1. Scattering force F_{scat}

Historically, the scattering force preceded full optical trapping in the form of Ashkin's levitation experiments [2–4]. It arises as a result of momentum transfer to a particle from incident photons as they are scattered from it.

A photon of light with frequency ν, wavelength λ and phase velocity v_{P} carries energy $E_{\mathrm{phot}} = h\nu = hv_{\mathrm{P}}/\lambda$ and momentum $p = h/\lambda = E_{\mathrm{phot}}/v_{\mathrm{P}}$. In absorbing a photon, an object therefore experiences a force $F_{\mathrm{scat}} = \partial p/\partial t = \partial(E_{\mathrm{phot}}/v_{\mathrm{P}})/\partial t = P/v_{\mathrm{P}} = nP/c$, where P is the power of the photon source. The last equality follows since the phase velocity of light in a material of refractive index n, $v_{\mathrm{P}} = c/n$, where c is the speed of light *in vacuo* [8, 9][1]. In our case, photons are scattered rather than absorbed and therefore transfer only a portion of their momentum to the particle; in the case of dielectric spheres, a prefactor $q \sim 0.1$ is customarily assumed [2, 9].

In our experiments, we have calculated F_{scat} to be on the order of a tenth of the particles' own weight for each mW of applied laser power (as measured at the laser, as always in this article); in a typical experiment this corresponds to around a tenfold increase in the particles' effective buoyant mass.

2.2. Gradient force F_{grad}

The gradient force F_{grad} allows a single beam, suitably focused, to act as an optical trap. Its origin is intuitively clear in the ray-optics formulation [9, 58], although since we ultimately consider the sum of forces over all infinitesimal volume elements of finite-sized spheres, we discuss the origin of the gradient force as it applies to Rayleigh particles. In this regime, the electric field over a particle is approximately uniform, and induces a dipole moment $\mathbf{p} = \alpha\mathbf{E}$, where α is the polarizability of the (dielectric) particle given by the Clausius–Mosotti relation [60]:

$$\alpha = n_{\mathrm{s}}^2 \left(\frac{n^2-1}{n^2+2}\right) a^3,$$

with $n = n_{\mathrm{c}}/n_{\mathrm{s}}$ the ratio of the refractive index of the colloidal particle, n_{c}, to that of the surrounding medium (solvent), n_{s}, and a the particle's radius. Having acquired a dipole moment, the particle experiences a Lorentz force $\mathbf{f}_{\mathrm{L}} = (\mathbf{p}\cdot\nabla)\mathbf{E} + (1/c)\mathrm{d}\mathbf{p}/\mathrm{d}t \times \mathbf{B}$. This can be re-written [55]:

$$\mathbf{f}_{\mathrm{L}} = \alpha\left(\nabla\left(\frac{1}{2}E^2\right) + \frac{1}{c}\frac{\partial}{\partial t}(\mathbf{E}\times\mathbf{B})\right).$$

The second term is the scattering force F_{scat} discussed above, and is directed along the direction of propagation. The first term, $F_{\mathrm{grad}} = (\alpha/2)\nabla E^2$, is the gradient force and expresses that in a non-uniform electric field, a particle will move towards regions of higher electric field if $n_{\mathrm{c}} > n_{\mathrm{s}}$, and vice versa. This indicates that the modulated potentials we seek can be realized by spatially modulated electric fields.

[1] We have assumed the Minkowski form, which differs from the Abraham form by a factor n^2. Although an important unresolved theoretical issue [59], this subtlety does not concern us unduly, since optical forces can be calibrated experimentally (and $n^2 \sim 1$).

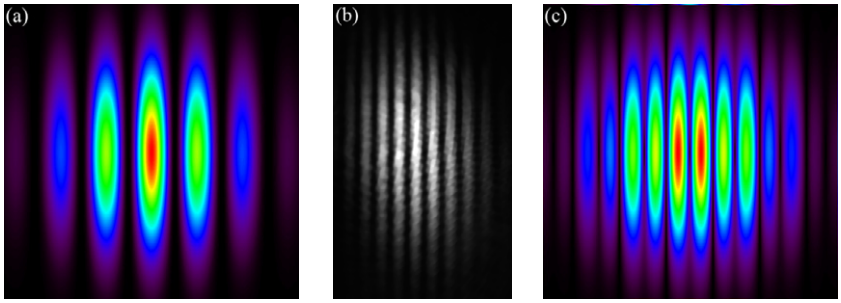

Figure 1. Fringe pattern calculated for typical experimental parameters which result in a fringe spacing $d = 9.29\ \mu$m (a), an observed fringe pattern (b), and the magnitude of the gradient force calculated based on the fringe pattern shown on the left (c). Parameters are (section 3.1): wavelength $\lambda = 532$ nm, crossing angle $\theta = 3.28°$, beam radius at the sample $R = 1.22\lambda f/D = 23.2\ \mu$m [21] for a laser beam of diameter $D = 2.80$ mm focused by a lens of focal length $f = 200$ mm.

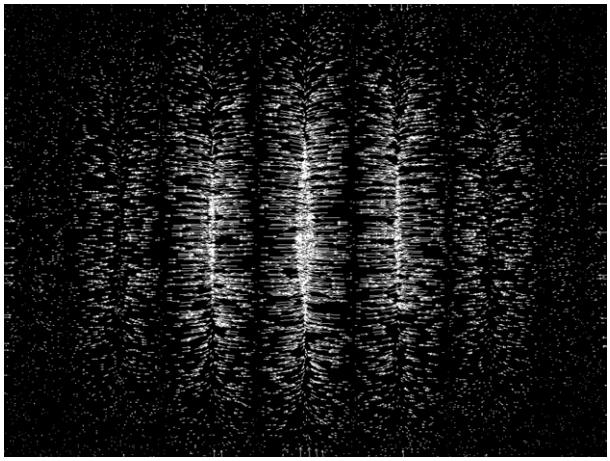

Figure 2. A vector plot showing the position-dependent force experienced by a particle, found by numerical differentiation (see the appendix) of the calculated pattern in figure 1(a).

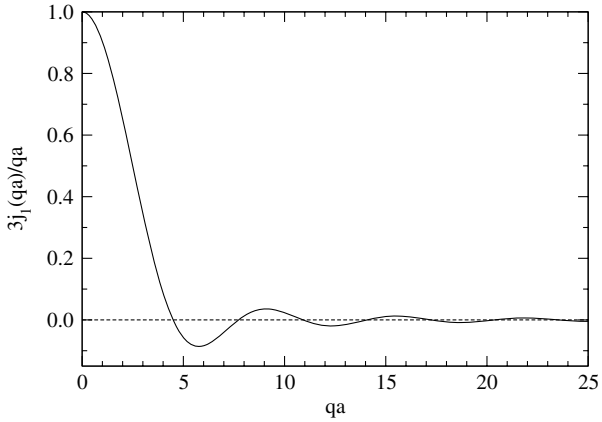

Figure 3. The factor $3j_1(qa)/(qa)$ arising from the finite particle radius a (equation (2)).

2.3. Modulated potentials from modulated light fields

One conceptually simple means of generating modulated light fields is using a crossed beam experiment, as employed in previous studies similar to ours [22, 33], and in thermal diffusion forced Rayleigh scattering studies [61, 62]. The experimental arrangement is also similar to the so-called 'dual-scatter' or 'dual-beam' configurations used in laser Doppler anemometry [63, 64]. For two crossed coherent TEM_{00} mode (Gaussian profile) laser beams, the resulting intensity profile is [24]:

$$I(x) = 2\,I_0\,\left\{1 + \cos\left[2kx\,\sin(\theta/2)\right]\right\}\,\mathrm{e}^{-2x^2\cos^2(\theta/2)/R^2} \qquad (1)$$

where θ is the beam crossing angle, I_0 the intensity of each beam, R the laser beam radius (the e^{-2} point), and $k = 2\pi/\lambda$ the incident beam wavevector. The term in braces, $\{1 + \cos[2kx\,\sin(\theta/2)]\} = \{1 + \cos[qx]\}$, is the sinusoidally-varying interference pattern of fringe spacing $d = \lambda/(2\sin(\theta/2))$ and fringe wavevector $q = 2\pi/d$. The last term represents the overlying Gaussian envelope due to the finite beam size. Figure 1 compares a calculated fringe pattern (a) with an experimentally observed pattern (b). From the gradient, the magnitude of the force can be calculated i.e. $F_{\mathrm{grad}} = (\alpha/2)\nabla E^2$ (c). These images illustrate that not only are particles drawn to the fringes, but they are also confined by the Gaussian envelope. Figure 2 illustrates this in the form of a vector field plot, which was obtained by numerical differentiation (see the appendix).

From the first term of the modulated light field, equation (1), we obtain the oscillatory part of the potential: $V(x) = V_0\{1 + \cos[qx]\}$, where V_0 absorbs the particles' polarizability and the laser beam intensity. Loudiyi *et al* additionally normalize this quantity by the thermal energy [24].

2.4. Effect of finite particle size

Implicit in all of the previous section was that the potential acts only at the centre of the particles, or alternatively that the particle radius $a \ll d$. This is not satisfied in the present work. For finite particle size, integration over infinitesimal volume elements of the particle results in a modified potential [24]:

$$V(x) = V_0\left\{1 + 3\frac{j_1(qa)}{qa}\cos\left[qx\right]\right\}\,, \qquad (2)$$

where x is the position of the particle centre and j_1 the first order spherical Bessel function.

The finite size of the particles leads to the additional factor $3j_1(qa)/(qa)$ (figure 3). This factor resembles the form

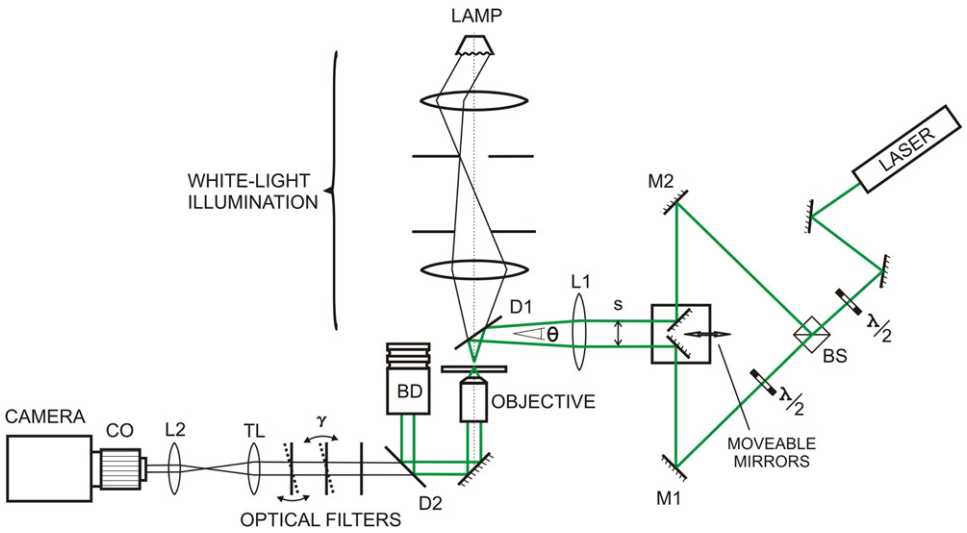

Figure 4. Schematic diagram of the experimental arrangement used to generate a modulated light field and simultaneously image the sample. Two coherent beams are created by beamsplitter BS, and subsequently brought parallel by two mirrors (M1, M2) and a pair of moveable mirrors. The position of the moveable mirrors determines the beam separation s, and therefore the beam crossing angle θ following focusing lens L1. For observation, white illuminating light is combined from above using dichroic mirror D1 and the sample imaged by an objective. The majority of the intense laser light is deflected to beam dump BD using a second dichroic mirror D2. A series of three optical filters, some rotatable, in the objective infinity space allows for variable attenuation of the remaining laser light and thus for an adjustment of the brightness of the fringes to be viewed. Images are recorded, after suitable magnification, using a digital camera.

factor of a sphere as it occurs in scattering experiments [65]. In a scattering experiment, the sample is illuminated by a beam and the intensity scattered under a scattering angle θ or, equivalently, a scattering vector q is determined. This implies an identical geometry with the incident and scattered beam here represented by the two crossing beams.

The additional factor demonstrates several interesting features [66]. First, for large fringe spacing ($qa \simeq 0$), the particles behave like point particles. Conversely, for very small fringe spacing ($qa \to \infty$), the effective potential is averaged to zero. Interestingly, there are fringe spacings where the sign of the potential is reversed, indicating that spherical particles can be either drawn into the fringes or repelled from them, depending on qa. As long as the fringe spacing is greater than $d = 0.699 \times 2a$ (corresponding to $qa = 4.493$, the first root of $j_1(qa)$), the factor $3j_1(qa)/(qa) > 0$. This means that for fringe spacings larger than the particle diameter but still finite (and indeed slightly smaller too), the behaviour is qualitatively similar to that for point particles, albeit with reduced potency.

3. Experiment

3.1. Apparatus

Figure 4 shows the experimental arrangement used to create the modulated potential and, at the same time, observe the response of the sample. The modulated potential is created by splitting a linearly-polarized laser beam (Coherent Verdi V5 with $P = 5$ W, $\lambda = 532$ nm) and subsequently crossing the two beams. The beam is split using a 50:50 beamsplitter (BS) with a preceding half-wave plate ($\lambda/2$) to adjust the polarization for optimum performance of the beamsplitter. The two beams are brought parallel to one another by means of two mirrors (M1, M2) and a moveable pair of mirrors. Translation of the moveable mirrors adjusts the beam separation s and, after the focusing lens (L1), the crossing angle θ of the two beams. A half-wave plate ($\lambda/2$) in one of the beams allows rotation of the polarization of one beam with respect to the other, thereby controlling the amplitude of the interference fringes whilst maintaining a constant mean intensity and thus radiation pressure.

The introduction of the sample changes the crossing angle. For a typical sample cell (depth 170 μm) and fringe spacing (7 μm), the angle of incidence is reduced from $\theta_i/2 = \sin^{-1}(\lambda/2d) = 2.2°$ to $\theta_r/2 = \sin^{-1}(\sin(2.2°)/1.33) = 1.6°$, corresponding to change in the focal position of 170 μm $\times$ $(\tan(\theta_i/2)/\tan(\theta_r/2) - 1) \simeq 64$ μm. This is corrected by a linear translation of the lens L1 (figure 4). Note that despite the change in the crossing angle, the fringe spacing remains unchanged (since λ also changes upon entering the new medium).

Concurrently, the sample is imaged with a home-built inverted bright-field microscope. Köhler illumination is provided from above the sample. The extremely long working distance condensing lens provides sufficient space for a 'notch' dichroic mirror (D1), reflective in a narrow range around $\lambda = 532$ nm but otherwise transmitting in the visible. This dichroic mirror combines the imaging and modulated light at the sample. After the sample, a standard high numerical aperture microscope objective (Nikon $\times$100 PA VC, NA = 1.4) forms an image at infinity, before a tube lens (TL) and subsequent telescope (L2, CO) adjust the magnification as appropriate for the camera. Additional optics can be introduced straightforwardly into the (relatively long) so-called infinity space behind the objective. We use this to separate the intense laser light, damaging to the camera, from the

white imaging light. The bulk (≃98%) is deflected to a beam dump (BD) using a second dichroic mirror (D2). As well as eliminating safely the majority of the laser light, this light can be re-used, for example by retro-reflection, to achieve a counter-propagating arrangement whereby F_{scat} can be reduced independently of the laser intensity. Even after the second dichroic mirror, the intensity of the laser light is far too high for the camera. Three additional optical filters are used to adjust the level of the modulated light field while retaining most of the imaging light. This permits simultaneous imaging of the sample and an appropriate fraction of the light field.

The intense laser light has to be reduced to about 10^{-9}–10^{-8} W at the camera, to obtain satisfactory images of the fringes. The fringes become essentially invisible upon a further reduction by a factor of about 100. Since the laser power varies depending on the experiment, for optimum simultaneous imaging, filters with a variable optical density at 532 nm, OD_{532}, are desirable. This can be achieved for interference filters by changing the angle of incidence, γ (figure 4): the filters have a sharp transmittance edge slightly above 532 nm which shifts to lower wavelength as γ is increased (similar to notch filters [67]). Since the slope of the edge is finite, this provides control over OD_{532} (figure 5). When placed in the infinity space of the microscope, these filters can be straightforwardly rotated to allow the fringes to be imaged or not, as desired. The weak dependence of OD_{532} within $-5^\circ \lesssim \gamma \lesssim 5^\circ$ (figure 5) is important for imaging, since this range is slightly larger than the divergence in the infinity space of the microscope[2]. Nevertheless, for different parts of the field of view, the effective γ and thus OD_{532} is different, and hence an image of the fringes is no longer quantitatively correct. A correct image can, however, be obtained with $\gamma = 0^\circ$, or by using neutral density filters (in which case the white light is attenuated beyond usefulness). The bright-field images remain good since the transmittance of each filter at wavelengths $\lambda \neq 532$ nm is $T \simeq 0.9$.

3.2. Analysis

Having determined the particle coordinates [68, 69], a range of parameters can be calculated, for example the particle density ϕ, the pair correlation function $g(r)$, the mean coordination number $\langle z \rangle$, the distribution of coordination numbers $p(z)$, and bond-orientational order parameters, e.g. ψ_6 [70]. Calibration of distances, necessary for determining the fringe spacing as well as for structural analyses, is performed using a high-resolution microscope test slide (Richardson Test Slide, Model 80303) [69].

3.3. Samples

We have used polystyrene sulfate spheres of radius $a = 2\ \mu$m (Interfacial Dynamics Corporation) suspended in water.

[2] Light from the focal plane is focused at infinity, but, except for light originating from the point on the optical axis, is nonetheless divergent. The focal length of an objective is the microscope tube lens focal length (here about 200 mm) divided by its magnification (here 100). Together with the radius of the field of view (here about 125 μm), this results in a divergence in the infinity space of the microscope of around $\tan^{-1}(125\ \mu\mathrm{m}/2\ \mathrm{mm}) \simeq 3.6^\circ$.

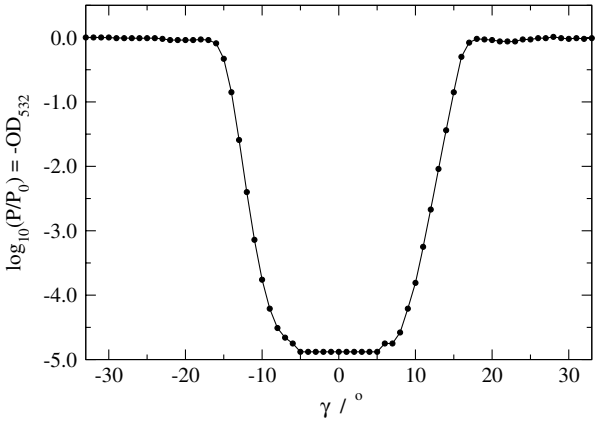

Figure 5. Variation of the filter optical density at 532 nm, OD_{532}, with the angle of incidence, γ. P_0 and P are the measured power values before and after the filters, respectively.

The large refractive index difference between particles ($n_{\mathrm{c}} = 1.59$) and water ($n_{\mathrm{s}} = 1.33$) results in large optical gradient forces, but the concomitant multiple scattering limits their use effectively to a single layer, i.e. two dimensions. These spheres carry negative charges, which in the present study are screened by high salt concentrations. We regard them as (almost) hard spheres, which is supported by the observed distance of closest approach and the shape of the pair correlation function (section 5.2). Though the salt concentration is high, it is still low enough to avoid problems with coagulation.

Samples are prepared by pipetting a suitably diluted homogenized stock solution directly into the sample cell, which fills largely by capillary action. The particles quickly sediment onto the coverglass. For dilute samples, this results in two-dimensional samples, while at higher concentrations a few layers form (which can be reduced to a single layer by application of radiation pressure, section 4). The concentrations we refer to in the following are the volume fractions ϕ of the initial, homogenized, bulk solutions. This is a nominal value; in the final sample, inhomogeneities in the density may occur depending on the settling process.

The sample cells consist of coverslips glued together, giving a sample volume of about 20 mm × 3 mm × 170 μm [69]. The sample only comes into contact with glass and possibly the UV-cure glue used to seal the cells, whose effect is assumed negligible. Since glass becomes negatively charged in the presence of water, the particles are repelled from the surfaces of the cell, and become attached only very occasionally [71, 72].

4. Radiation pressure results

We first investigate the effect of radiation pressure only as a function of laser intensity and particle concentration (figure 6). The radiation pressure is applied by turning the second half-wave plate ($\lambda/2$) until minimum contrast is achieved as judged from images of the interference patterns formed using neutral density filters. The concentrations are chosen such that a first layer of particles next to the coverslip (slightly out of focus in

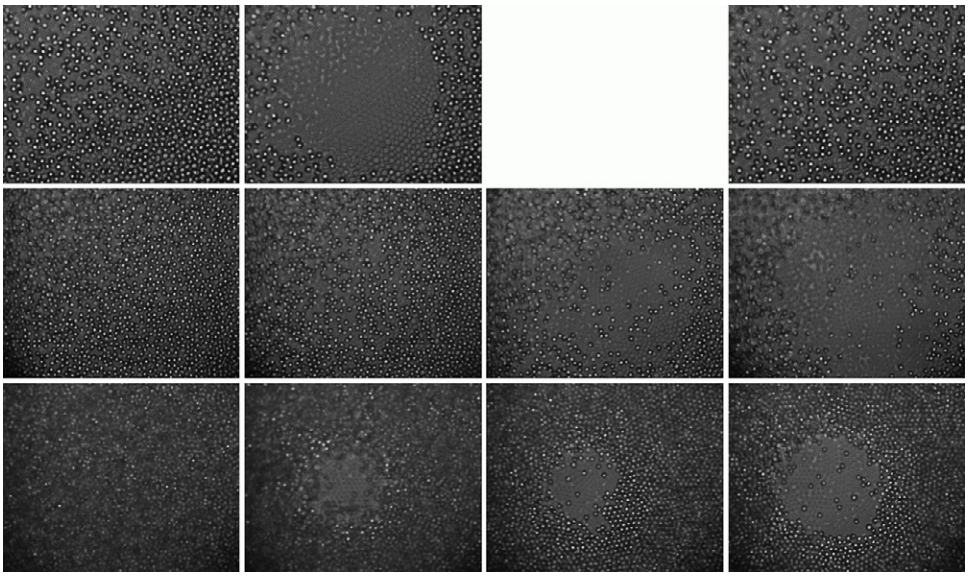

Figure 6. The effect of pure radiation pressure as a function of sample concentration (from top to bottom: initial homogenized volume fractions $\phi = 0.015$, 0.020, and 0.030) and laser intensity (left to right: $P = 0.00$, 0.10, 0.20, and 0.50 W). Images are taken following 20 min of irradiation, except for the top right image which shows the sample ($\phi = 0.015$, $P = 0.10$ W) 30 min after the laser is turned off. Note that only the particles in the second layer are in focus; they show a bright spot at their centre. Particles in the first layer (most prominent in the image second from left, top row) are out of focus but still clearly identifiable.

figure 6) as well as an incomplete second layer (in focus) are formed.

As the sample concentration increases (downwards in figure 6), the density of the second layer increases. The presence of a second layer does not imply that the maximum possible density has been achieved in the first layer. Indeed, this is observed not to be the case: upon increasing the radiation pressure, particles are pushed from the second layer into the first layer (left to right). In each of these cases the radiation pressure was applied for 20 min. In the least dense sample (top row), a laser intensity $P = 0.10$ W is already sufficient to insert all of the particles into the first layer. (The two highest laser intensity results for the lowest concentration are omitted in figure 6.) This forms a dense hexagonally-close packed (HCP) layer. With increasing density, a greater laser intensity is required to insert all of the particles within the laser beam into the first layer. Beyond a certain density, it is no longer possible to insert all of the particles into the first layer, even for very large radiation pressures. With increasing concentration, the area with only a single layer gets smaller, corresponding to the Gaussian profile of the laser beam and thus the applied radiation pressure. This can also be seen with increasing laser intensity.

The top rightmost image shows the least concentrated sample 30 min after the field is removed. (Similar relaxation behaviour is observed in all samples.) The second layer has become repopulated. This indicates that the osmotic pressure experienced within the highly concentrated first layer is sufficient to cause particles to 'pop up' into the second layer. This also implies that the inability of particles to enter the first layer under their own weight cannot be explained by pure geometrical frustration. We have observed that 'popping up' occurs with a characteristic time of about 10 s. If this upward movement into the second layer is thermally driven, i.e. is a chance Brownian excursion (and a return to the first layer is hindered by particle rearrangements within the first layer), its timescale should be given by Kramer's escape time with a ramp potential of depth U_0 and extent $2a$ representing the gravitational potential [49, 73]:

$$\tau = \frac{1}{D_s}\int_0^{2a} \mathrm{d}x' \, \mathrm{e}^{\beta U(x')} \int_{-\infty}^{x'} \mathrm{d}x \, \mathrm{e}^{-\beta U(x)} = \frac{(2a)^2}{D_s} \frac{\mathrm{e}^{-\beta U_0} - (1 - \beta U_0)}{(\beta U_0)^2},$$

where $\beta = 1/k_B T$ and D_s is the self-diffusion constant for a free particle. Using appropriate parameters gives $\tau \sim 10^6$ s $\gg$ 10 s, indicating the presence of a driving force, namely the osmotic pressure.

This seems plausible in light of the established connection between the statistical geometry of hard spheres and their thermodynamic properties [74–76]. These references suggest that insertion of particles into a disordered layer by the application of radiation pressure should, as in the Widom insertion method, permit study of the thermodynamic properties of particles in the first layer.

5. Modulated potential results

Having established a two-dimensional sample, we now introduce a modulated potential. In the present study, the modulation is always as great as possible at the specified laser intensity, i.e. both beams have the same direction of polarization. In each experiment, we prepare a dense hexagonally-close packed (HCP) layer using radiation pressure (at the indicated power) before the half-wave plate is rotated to 'turn on' the modulation. The parameters we vary are the

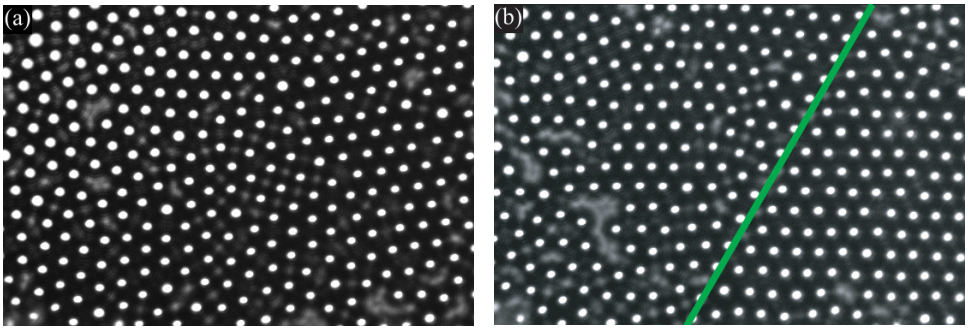

Figure 7. Sample (initial concentration $\phi = 0.020$) after 30 min of pure radiation pressure (a) followed by a further 30 min with a modulated potential of wavelength $d = \sqrt{3}a$ (b). The laser intensity in both cases is $P = 0.5$ W, and the superimposed line indicates the approximate fringe direction.

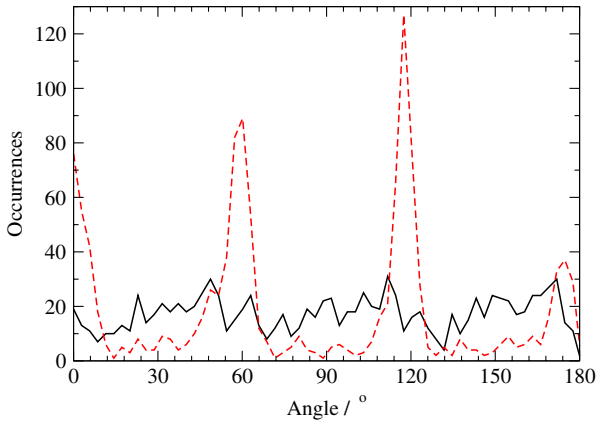

Figure 8. Distribution of the nearest-neighbour bond direction for a sample (initial concentration $\phi = 0.020$) after 30 min of pure radiation pressure (solid (black) line) followed by a further 30 min with a modulated potential of wavelength $d = \sqrt{3}a$ (dashed (red) line). The laser intensity is $P = 0.5$ W.

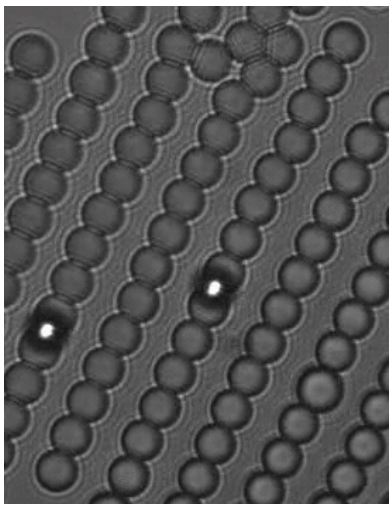

Figure 9. A dilute sample exposed to a modulated light field ($P = 0.50$ W) with spacing $d = 2\sqrt{3}a$.

fringe separation and the amplitude of the modulation. The HCP symmetry suggests a few fringe spacings d (figure 12(a)); here we investigate $d = \sqrt{3}a$ (section 5.1) and $d = 2\sqrt{3}a$ (section 5.2).

5.1. Natural fringe spacing

For a modulated potential of fringe spacing $d = \sqrt{3}a$, it is possible for all particles forming an HCP layer to lie at the potential minimum. We thus consider this a natural fringe spacing.

Pure radiation pressure (a single beam of $P = 0.50$ W for 30 min) leads to randomly-oriented crystallites (figure 7, left). After exposure to the modulated potential ($P = 0.50$ W for 30 min), the crystallites have rotated and consolidated to a near-perfect crystal with a clear direction aligned with the fringes (right). This is also reflected in the distribution of the nearest-neighbour bond direction, which shows three strong peaks separated by 60° (figure 8).

The crystallites thus seem to be able to rearrange despite the high density. It is interesting to investigate exactly how this process occurs. One observation is that as part of a crystallite rotates, the total energy in the light field does not decrease monotonically until the particles are aligned with the field. At some angles ψ between the light field and the crystal orientation, relatively many particles are near to the potential minima. When the particles are aligned with the field ($\psi = 0°$), all of the particle centres occupy a minimum. For angles $\psi \simeq 18°$, 31°, and 42°, there are only around 40%, 60%, and 40% of the particles in the minimum respectively, whereas for in-between angles there are far fewer. Supposing a large crystallite were to rotate towards the global minimum, therefore, it may do so at varying speed, perhaps even pausing at these intermediate metastable orientations depending on the amplitude of the field.

5.2. Twice natural fringe spacing

We now consider a fringe spacing $d = 2\sqrt{3}a$ corresponding to twice the spacing between two rows of an HCP layer. For sufficiently dilute samples, the particles align along the fringes (figure 9).

In dense samples, more complex structures develop (figure 10). The initially disordered sample (top left) develops

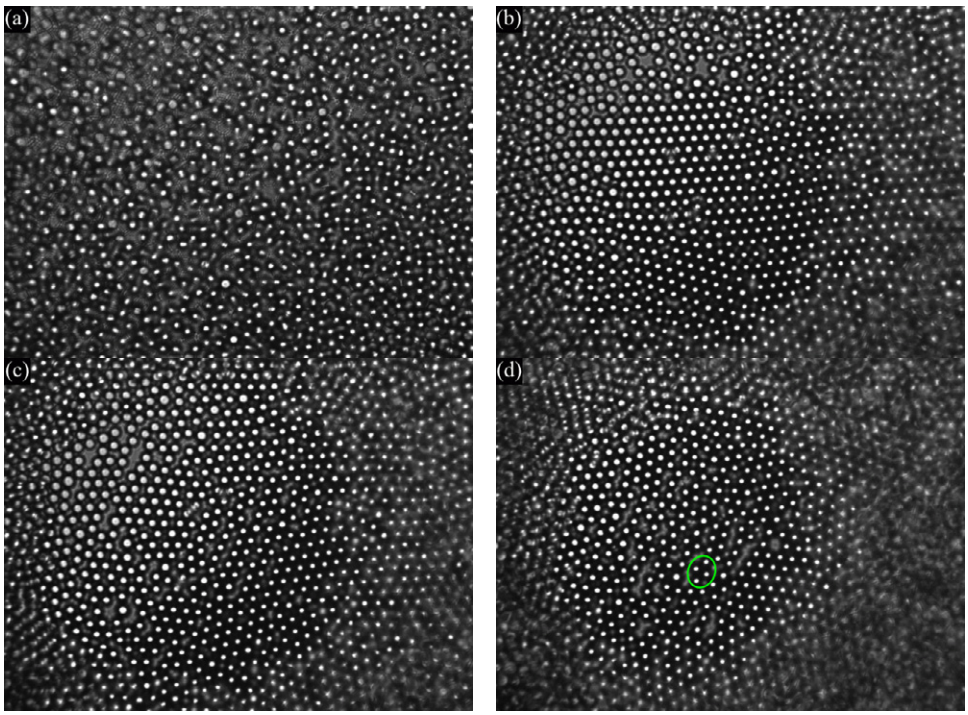

Figure 10. Micrographs of a sample (initial concentration $\phi = 0.020$) before irradiation (a), following 1 h of radiation pressure at a laser intensity of $P = 0.40$ W (b), and 100 s (c) and about 5 h (d) after the introduction of fringes with spacing $d = 2\sqrt{3}a$.

randomly-oriented crystallites following the application of radiation pressure (1 h of $P = 0.40$ W, top right), as described previously (section 4). Relatively soon after a modulation of wavelength $d = 2\sqrt{3}a$ is introduced (100 s, still with $P = 0.40$ W, bottom left), the sample is altered, with the emergence of voids which run broadly in the direction of the fringes. After substantially more time (about 5 h, bottom right), the field has caused significant structural rearrangement. In time-lapse movies of images, groups of clusters can be seen moving co-operatively, leading to arrangements along the potential minima. In particular, the motif highlighted in figure 10 (bottom right) occurs frequently, with an orientation relative to the fringes as indicated in figure 12(d). This rotation is understandable on energetic grounds, which we discuss further below. Other samples show similar behaviour.

The structural evolution of the sample has been investigated more quantitatively by following the rearrangements induced by a modulated potential (figure 11). We determined the positions of particles which were located in a rectangular region within the single-layer region and thus under the influence of the modulated potential. Over the course of the whole period, the number of particles $N(t)$ within the observation region and thus the particle density steadily decreases (figure 11(a)). In addition, a particle's average number of neighbours $\langle z(t)\rangle$ drops from around 4.4 to 3.9 after 3.5 h (figure 11(b)). This is also reflected in the distribution of the number of neighbours $p(z, t)$ (figure 11(c)), which indicates an increasing probability of weakly connected particles, consistent with the appearance of voids along the fringes. Although the number of neighbours decreases, the bond-orientational order parameter ψ_6 (section 3.2) does not change significantly over the course of the experiment (figure 11(d)). This indicates that those particles which remain bonded do so in a morphologically similar way. This is supported by the fact that the pair correlation function $g(r)$ is also essentially unaffected throughout the experiment (figure 11(e)).

How can we understand these observations? In dilute samples, all of the particles can be arranged in the potential minima. For the dense samples, half of the particles can still lie along the minima (figure 12(a)) (section 5.1), but the remaining particles are forced to lie between the fringes and thus at the maximum of the potential. While the intensity gradient and hence the force is zero at the maximum, this arrangement is metastable, with very small fluctuations inevitably resulting in large gradient forces. These forces attempt to insert particles into the minima, i.e. the fringes (two such particles are indicated as blue rings in figure 12(b)), and in so doing push other particles along the fringes (as indicated by the arrows in the right-hand image in figure 12(b)). This is achieved without penalty, provided the density at the end of the fringe is suitably low. When the density of the sample is large, there is a significant osmotic penalty associated with pushing particles along the fringes and into the bulk. A balance must be struck between the optical gradient force and the osmotic force, which are opposed in their preference for density modulations. This explains why the expected modulations in density are observed at low concentrations (figure 9), but not at very high concentrations. At high densities, the system aims to accommodate as many particles as possible within the fringe, without significant extension along the fringe. We have observed structures which achieve this; one example is that highlighted in figure 10 (bottom right) and

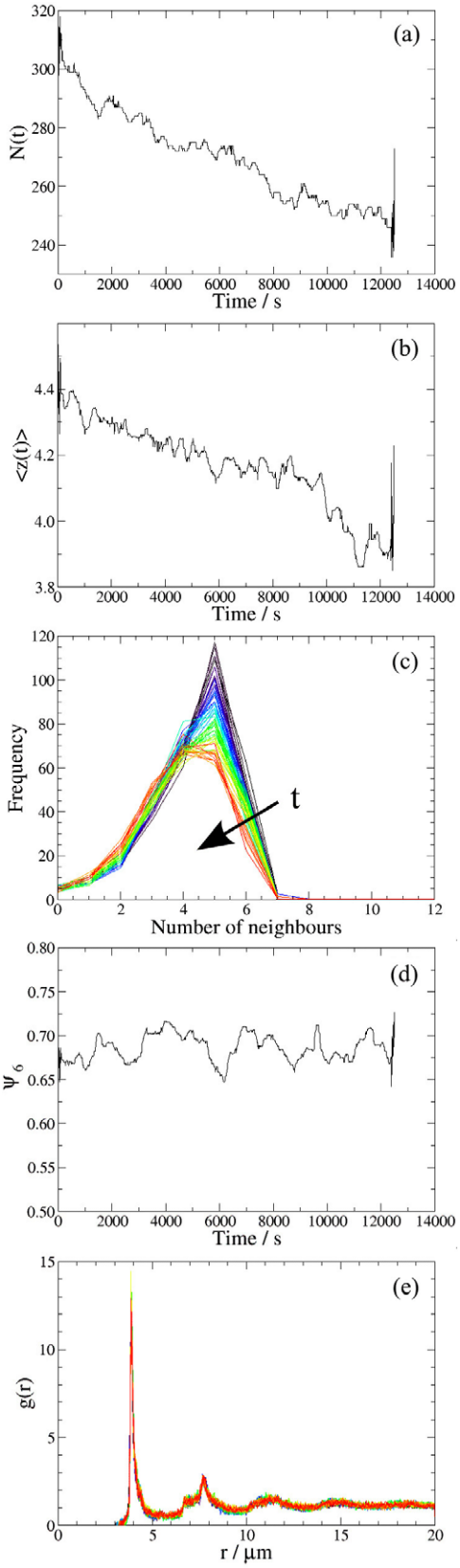

Figure 11. Effect of a modulated potential on the evolution of different parameters. Shown are the time dependence of (a) the number of particles $N(t)$ within the observation region, (b) the average number of neighbours $\langle z(t)\rangle$, (c) the distribution of the number of neighbours $p(z, t)$ with time (direction of increasing time indicated by arrow), (d) the bond-orientational order parameter $\psi_6(t)$, and (e) the pair correlation function $g(r, t)$.

explained in figure 12(d). This rhombic 'motif' represents a part of the crystal which, after rotation through 30°, reaches an energetically advantageous state (which depends on the precise details of the potential, see below) without a large extension along the fringe direction. The rearrangement of small crystalline parts leaves bond orientations unchanged, consistent with the observed essentially constant ψ_6, as well as leaving inter-particle distances largely unchanged. This latter observation is consistent with our finding that $g(r)$ does not change substantially. What modest extension along the fringes there is expels some particles, in agreement with the decrease in the particle number $N(t)$ and in turn the mean number of neighbours $\langle z(t)\rangle$.

These observations might have interesting consequences. First, if what we observe are equilibrium structures, it is remarkable that they form via small crystalline parts which are broken away and simply reoriented with respect to the applied potential. It is, however, also conceivable that, due to the geometrical frustration in a dense system, these co-operative motions are the only means by which the system can rearrange. In this case, the observed structures would correspond to non-equilibrium states liable to further evolution; indeed the evolution of particle number $N(t)$ and mean coordination number $\langle z(t)\rangle$ suggests that the samples are still evolving (figures 11(a), (b)). Whether equilibrium or not, it is clear that the modulated potential has a profound effect even in these dense samples. Our experiments also suggest that at intermediate (in the present context, though these are still relatively very dense samples) concentrations, novel structures might form due to the competition between the imposed potential which favours density modulations, and the osmotic pressure of the system which opposes them.

Which structure is energetically or kinetically preferable depends on the shape of the potential. For example, for a square-well potential, the particles can, to some extent, move laterally within the fringe without penalty. Depending on the potential width and separation, a wealth of structures has been predicted for this case [77]. Although in that study the colloids remain near to one another due to mutual attraction rather than osmotic pressure (as in our case), the effect is seemingly similar. For a potential with monotonically increasing curvature, e.g. a quadratic potential, it is advantageous to displace particles from the minimum as little as possible; 'zig-zag' lines are expected. In the present case, however, the curvature of the potential is non-monotonic and it seems reasonable that some particles maintain their position while others are significantly displaced from the potential minimum. Together with the influence of the osmotic pressure due to the bulk sample, this energy-minimization argument justifies the existence of the observed motifs.

6. Conclusion

We have described an apparatus used to expose a sample to sinusoidally-varying light fields and simultaneously image the sample. To demonstrate its capabilities, we have investigated the response of colloidal particles to the modulated potentials which arise from the light field. We have shown that

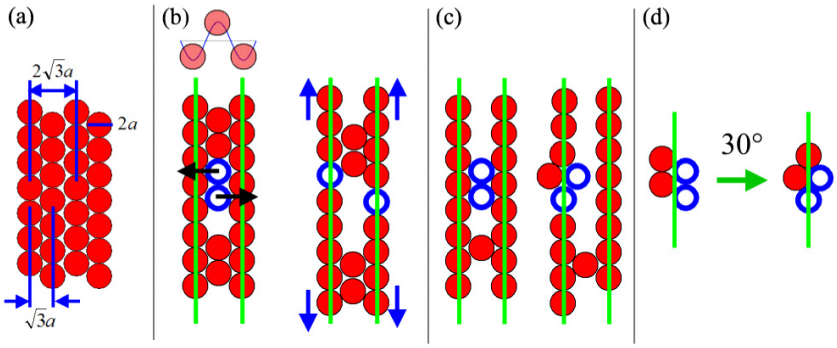

Figure 12. (a) Hexagonally-close packed (HCP) layer of particles with radius a and inter-layer spacing $\sqrt{3}a$. (b) Particles located along the fringes (minima) are stable while those at the maxima (two of which are shown in the figure as blue rings) are metastable and, as a result of fluctuations, experience a force toward the fringes. They can join a minimum if particles which are already present in the minimum can advance along it (arrows in the right-hand image). (c) When this is hindered, the particles can locally rearrange (e.g., rotate by 30°) to adopt more favourable structures.

these potentials influence even samples dense enough that the dynamics of their constituent particles are severely restricted. Currently we are further improving the apparatus by including a counter-propagating beam which will allow us to control the modulated potential and radiation pressure independently. This will be achieved by replacing the beam dump by a retro-reflector.

Densely packed effectively two-dimensional samples have been generated using radiation pressures of different intensity. The behaviour of these samples upon exposure to modulated potentials has been investigated for two different modulation wavelengths. This has revealed co-operative structural rearrangements and final structures which seem to result from a competition between the optical gradient force and the osmotic pressure of the bulk sample. While theoretical predictions for a sinusoidal potential are lacking, similar theoretical calculations suggest structures comparable to those we have observed.

With this apparatus, we can now investigate different situations: first, for disorder-to-order transitions, specific predictions exist for binary hard disc mixtures under similar conditions to those described here [42]. Second, disorder-to-disorder transitions are expected for systems with attractive interactions exposed to modulated potentials [40]. Both these transitions represent reversible transitions starting from equilibrium states, in which the initial states are recovered on removal of the modulated potential. In contrast, in a third situation, high-density non-equilibrium systems, in particular repulsive and attractive glasses, might undergo irreversible transitions from their non-equilibrium state to an ordered equilibrium state upon exposure to a modulated potential. In this case, structural rearrangements lead to stable configurations that persist even after removal of the external potential. In addition to revealing new physics, this might also have implications for material sciences.

Acknowledgments

We thank Hartmut Löwen, Wilson Poon and Richard Hanes for helpful discussions. We also thank Jürgen Liebetrau for technical assistance and Beate Moser for help in preparing the diagrams. This work was funded by the Deutsche Forschungsgemeinshaft (DFG) within the German–Dutch Collaborative Research Centre Sonderforschungsbereich-Transregio 6 (SFB-TR6), Project Section C7.

Appendix. Numerical differentiation of patterns

The calculated intensity profile was differentiated numerically using the Sobel method [78, section 7.1.3] to obtain an approximation to the force field experienced by the particles. If f is the image, then the gradient of the image

$$\nabla \mathbf{f} = \begin{bmatrix} G_x \\ G_y \end{bmatrix} = \begin{bmatrix} \partial f/\partial x \\ \partial f/\partial y \end{bmatrix},$$

with magnitude $|\nabla \mathbf{f}| = (G_x^2 + G_y^2)^{1/2}$ and direction $\varphi(x, y) = \tan^{-1}(G_y/G_x)$ is formed by convolution of the image with the following kernels:

$$G_x = \begin{array}{|c|c|c|}\hline -1 & -2 & -1 \\ \hline 0 & 0 & 0 \\ \hline 1 & 2 & 1 \\ \hline \end{array} \qquad G_y = \begin{array}{|c|c|c|}\hline -1 & 0 & 1 \\ \hline -2 & 0 & 2 \\ \hline -1 & 0 & 1 \\ \hline \end{array}$$

References

[1] Haw M D 2002 Colloidal suspensions, Brownian motion, molecular reality: a short history *J. Phys.: Condens. Matter* **14** 7769–79
[2] Ashkin A 1970 Acceleration and trapping of particles by radiation pressure *Phys. Rev. Lett.* **24** 156–9
[3] Ashkin A and Dziedzic J M 1971 Optical levitation by radiation pressure *Appl. Phys. Lett.* **19** 283–5
[4] Ashkin A and Dziedzic J M 1974 Stability of optical levitation by radiation pressure *Appl. Phys. Lett.* **24** 586–8
[5] Ashkin A 1980 Applications of laser radiation pressure *Science* **210** 1081–8
[6] Smith P W, Ashkin A and Tomlinson W J 1981 Four-wave mixing in an artificial Kerr medium *Opt. Lett.* **6** 284–6
[7] Ashkin A, Dziedzic J M and Smith P W 1982 Continuous-wave self-focusing and self-trapping of light in artificial Kerr media *Opt. Lett.* **7** 276–8
[8] Ashkin A, Dziedzic J M, Bjorkholm J E and Chu S 1986 Observation of a single-beam gradient force optical trap for dielectric particles *Opt. Lett.* **11** 288–90
[9] Molloy J E and Padgett M J 2002 Lights, action: optical tweezers *Contemp. Phys.* **43** 241–58

[10] Svoboda K and Block S M 1994 Biological applications of optical forces *Annu. Rev. Biophys. Biomol. Struct.* **23** 247–85
[11] Sheetz M P 1998 *Laser Tweezers in Cell Biology (Methods in Cell Biology)* (New York: Academic)
[12] Greulich K O 1999 *Micromanipulation by Light in Biology and Medicine* (Berlin: Springer)
[13] Pusey P N 1991 *Liquids, Freezing and Glass Transition* (Amsterdam: Elsevier) chapter 10 (Colloidal Suspensions) pp 763–942
[14] Poon W C-K 2002 The physics of a model colloid–polymer mixture *J. Phys.: Condens. Matter* **14** R859–80
[15] Pusey P N and van Megan W 1986 Phase behaviour of concentrated suspensions of nearly hard colloidal spheres *Nature* **320** 340–2
[16] Pusey P N and van Megan W 1987 Observation of a glass transition in suspensions of spherical colloidal particles *Phys. Rev. Lett.* **59** 2083–6
[17] van Megen W and Underwood S M 1993 Dynamic-light-scattering study of glasses of hard colloidal spheres *Phys. Rev.* E **47** 248–61
[18] Weeks E R, Crocker J C, Levitt A C, Schofield A B and Weitz D A 2000 Three-dimensional direct imaging of structural relaxation near the colloidal glass transition *Science* **287** 627–31
[19] Ferrer M L, Lawrence C, Demirjian B G, Kivelson D, Alba-Simionesco C and Tarjus G 1998 Supercooled liquids and the glass transition: temperature as the control variable *J. Chem. Phys.* **109** 8010–5
[20] Härtl W, Versmold H and Zhang-Heider X 1995 The glass transition of charged polymer colloids *J. Chem. Phys.* **102** 6613–8
[21] Chowdhury A H 1986 Laser induced freezing *PhD Thesis* Oklahoma State University
[22] Chowdhury A and Ackerson B J 1985 Laser-induced freezing *Phys. Rev. Lett.* **55** 833–7
[23] Ackerson B J and Chowdhury A H 1987 Radiation pressure as a technique for manipulating the particle order in colloidal suspensions *Faraday Discuss. Chem. Soc.* **83** 309–16
[24] Loudiyi K and Ackerson B J 1992 Direct observation of laser induced freezing *Physica* A **184** 1–25
[25] Loudiyi K and Ackerson B J 1992 Monte Carlo simulation of laser induced freezing *Physica* A **184** 26–41
[26] Wei Q-H, Bechinger C, Rudhardt D and Leiderer P 1998 Structure of two-dimensional colloidal systems under the influence of an external modulated light field *Prog. Colloid Polym. Sci.* **110** 46–9
[27] Xu H and Baus M 1986 Freezing in the presence of a periodic external potential *Phys. Lett.* A **117** 127–31
[28] Barrat J L and Xu H 1990 The phase diagram of hard spheres in a periodic external potential *J. Phys.: Condens. Matter* **2** 9445–50
[29] Chakrabarti J, Krishnamurthy H R and Sood A K 1994 Density functional theory of laser-induced freezing in colloidal suspensions *Phys. Rev. Lett.* **73** 2923–6
[30] Sood A K 1996 Some novel states of colloidal matter: modulated liquid, modulated crystal and glass *Physica* A **224** 34–47
[31] Chakrabarti J, Krishnamurthy H R, Sood A K and Sengupta S 1995 Reentrant melting in laser field modulated colloidal suspensions *Phys. Rev. Lett.* **75** 2232–5
[32] Wei Q-H, Bechinger C, Rudhardt D and Leiderer P 1998 Experimental study of laser-induced melting in two-dimensional colloids *Phys. Rev. Lett.* **81** 2606–9
[33] Bechinger C, Wei Q H and Leiderer P 2000 Reentrant melting of two-dimensional colloidal systems *J. Phys.: Condens. Matter* **12** A425–30
[34] Bechinger C, Brunner M and Leiderer P 2001 Phase behavior of two-dimensional colloidal systems in the presence of periodic light fields *Phys. Rev. Lett.* **86** 930–3
[35] Bechinger C and Frey E 2001 Phase behaviour of colloids in confining geometry *J. Phys.: Condens. Matter* **13** R321–36
[36] Bechinger C 2002 Colloidal suspensions in confined geometries *Curr. Opin. Colloid Interface Sci.* **7** 204–9
[37] Strepp W, Sengupta S and Nielaba P 2001 Phase transitions of hard disks in external potentials: a Monte Carlo study *Phys. Rev.* E **63** 046106
[38] Strepp W, Sengupta S and Nielaba P 2002 Phase transitions of soft disks in external potentials: a Monte Carlo study *Phys. Rev.* E **66** 056109
[39] Strepp W, Sengupta S, Lohrer M and Nielaba P 2002 Phase transitions of hard and soft disks in external periodic potentials: a Monte Carlo study *Comput. Phys. Commun.* **147** 370–3
[40] Götze I O, Brader J M, Schmidt M and Löwen H 2003 Laser-induced condensation in colloid–polymer mixtures *Mol. Phys.* **101** 1651–8
[41] Rex M, Löwen H and Likos C N 2005 Soft colloids driven and sheared by traveling wave fields *Phys. Rev.* E **72** 021404
[42] Franzrahe K and Nielaba P 2007 Entropy versus energy: the phase behavior of a hard-disk mixture in a periodic external potential *Phys. Rev.* E **76** 061503
[43] Pham K N, Puertas A M, Bergenholtz J, Egelhaaf S U, Moussaïd A, Pusey P N, Schofield A B, Cates M E, Fuchs M and Poon W C K 2002 Multiple glassy states in a simple model system *Science* **296** 104–6
[44] Götze W and Sjogren L 1992 Relaxation processes in supercooled liquids *Rep. Prog. Phys.* **55** 241–376
[45] Ackerson B J and Pusey P N 1988 Shear-induced order in suspensions of hard spheres *Phys. Rev. Lett.* **61** 1033–6
[46] Haw M D, Poon W C K, Pusey P N, Hebraud P and Lequeux F 1998 Colloidal glasses under shear strain *Phys. Rev.* E **58** 4673–82
[47] Haw M D, Poon W C K and Pusey P N 1998 Direct observation of oscillatory-shear-induced order in colloidal suspensions *Phys. Rev.* E **57** 6859–64
[48] Vermant J and Solomon M J 2005 Flow-induced structure in colloidal suspensions *J. Phys.: Condens. Matter* **17** R187–216
[49] Smith P A, Petekidis G, Egelhaaf S U and Poon W C K 2007 Yielding and crystallization of colloidal gels under oscillatory shear *Phys. Rev.* E **76** 041402
[50] Besseling R, Weeks E R, Schofield A B and Poon W C K 2007 Three-dimensional imaging of colloidal glasses under steady shear *Phys. Rev. Lett.* **99** 028301
[51] Koumakis N, Schofield A B and Petekidis G 2008 Effects of shear-induced crystallization on the rheology and ageing of hard sphere glasses *Preprint* 0804.1218
[52] Ackerson B J and Clark N A 1981 Shear-induced melting *Phys. Rev. Lett.* **46** 123–7
[53] Stevens M J, Robbins M O and Belak J F 1991 Shear melting of colloids: a nonequilibrium phase diagram *Phys. Rev. Lett.* **66** 3004–7
[54] Biroli G, Bouchaud J-P, Miyazaki K and Reichman D R 2006 Inhomogeneous mode-coupling theory and growing dynamic length in supercooled liquids *Phys. Rev. Lett.* **97** 195701
[55] Gordon J P 1973 Radiation forces and momenta in dielectric media *Phys. Rev.* A **8** 14–21
[56] Harada Y and Asakura T 1996 Radiation forces on a dielectric sphere in the Rayleigh scattering regime *Opt. Commun.* **124** 529–41
[57] Tlusty T, Meller A and Bar-Ziv R 1998 Optical gradient forces of strongly localized fields *Phys. Rev. Lett.* **81** 1738–41
[58] Ashkin A 1992 Forces of a single-beam gradient laser trap on a dielectric sphere in the ray optics regime *Biophys. J.* **61** 569–82
[59] Leonhardt U 2006 Momentum in uncertain light *Nature* **444** 823–4
[60] Jackson J D 1975 *Classical Electrodynamics* 2nd edn (New York: Wiley)

[61] Wiegand S 2004 Thermal diffusion in liquid mixtures and polymer solutions *J. Phys.: Condens. Matter* **16** R357–79
[62] Köhler W and Schäfer R 2000 Polymer analysis by thermal-diffusion forced Rayleigh scattering *Adv. Polym. Sci.* **151** 1–59
[63] Brayton D B and Goethert W H 1971 A new dual-scatter laser Doppler-shift velocity measuring technique *ISA Trans.* **10** 40–50
[64] Durst F, Melling A and Whitelaw J H 1976 *Principles and Practice of Laser-Doppler anemometry* (New York: Academic)
[65] Lindner P and Zemb T (ed) 2002 *Neutrons, X-rays and Light: Scattering Methods Applied to Soft Condensed Matter* (Amsterdam: Elsevier)
[66] Chowdhury A H, Wood F K and Ackerson B J 1991 Transverse radiation pressure forces for finite sized colloidal particles *Opt. Commun.* **86** 547–54
[67] Semrock Inc. Notch filter spectra versus angle of incidence http://www.semrock.com/Catalog/Notch_SpectrumvsAOI.htm (obtained March 2008)
[68] Crocker J C and Grier D G 1996 Methods of digital video microscopy for colloidal studies *J. Colloid Interface Sci.* **179** 298–310
[69] Jenkins M C and Egelhaaf S U 2008 Confocal microscopy of colloidal particles: towards reliable, optimum coordinates *Adv. Colloid Interface Sci.* **136** 65–92
[70] de Villeneuve V W A, Dullens R P A, Aarts D G A L, Groeneveld E, Scherff J H, Kegel W K and Lekkerkerker H N W 2005 Colloidal hard-sphere crystal growth frustrated by large spherical impurities *Science* **309** 1231–3
[71] Prieve D C and Loo F 1987 Brownian motion of a hydrosol particle in a colloidal force field *Faraday Discuss. Chem. Soc.* **83** 297–307
[72] Prieve D C 1999 Measurement of colloidal forces with TIRM *Adv. Colloid Interface Sci.* **82** 93–125
[73] Kramers H A 1940 Brownian motion in a field of force and the diffusion model of chemical reactions *Physica* **7** 284–304
[74] Dullens R P A, Aarts D G A L and Kegel W K 2006 Direct measurement of the free energy by optical microscopy *Proc. Natl Acad. Sci. USA* **103** 529–31
[75] Dullens R P A, Aarts D G A L, Kegel W K and Lekkerkerker H N W 2005 The Widom insertion method and ordering in small hard-sphere systems *Mol. Phys.* **103** 3195–200
[76] Widom B 1963 Some topics in the theory of fluids *J. Chem. Phys.* **39** 2808–12
[77] Harreis H M, Schmidt M and Löwen H 2002 Decoration lattices of colloids adsorbed on stripe-patterned substrates *Phys. Rev.* E **65** 041602
[78] Gonzalez R C and Woods R E 1992 *Digital Image Processing* (Reading, MA: Addison-Wesley)